Food Hydrocolloids 126 (2022) 107473

Contents lists available at ScienceDirect

Food Hydrocolloids

journal homepage: www.elsevier.com/locate/foodhyd

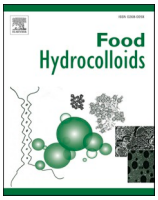

Meta-analysis of critical points to determine second virial coefficients for binary biopolymer mixtures

Arjen Bot [a,b], Belinda P.C. Dewi [a], Titia Kool [a], Erik van der Linden [a], Paul Venema [a,*]

[a] Laboratory of Physics and Physical Chemistry of Foods, Wageningen University and Research, Bornse Weilanden 9, 6708 WG Wageningen, the Netherlands
[b] Unilever Foods Innovation Centre, Bronland 14, 6708 WH Wageningen, the Netherlands

ARTICLE INFO

Keywords:
Phase separation
Phase diagram
Meta-analysis
Critical point
Edmond-Ogston
Model
Second virial coefficient

ABSTRACT

A method is introduced to extract virial coefficients from phase diagrams. Previous work demonstrated that the critical point of a phase diagram (two parameters) of a binary polymer mixture provides too little information to allow a full description of the phase diagram when using the Edmond-Ogston model (which requires three parameters). In this paper, it is shown that simultaneous analysis of multiple phase diagrams of binary polymer mixtures with shared components does allow the extraction of virial coefficients. The method is illustrated by analyzing phase diagrams for various polymer mixtures directly available in literature. The obtained virial coefficients for the polyethylene oxide/polyethylene glycol (PEO) and dextran polymers are compared to values as obtained by membrane osmometry and shown to be in satisfactory agreement. These virial coefficients are shown to follow a power-law dependence on the molecular weight. In addition, it is observed that the cross-virial coefficient can be approximately described by a simple mixing rule. This rule makes it possible to estimate the phase diagrams for polymer mixtures, where the virial coefficients of the pure components are known, but the cross-virial coefficient is unknown. The method to extract virial coefficients is also applied to a number of mixtures containing agarose, bovine serum albumin or gelatin, mixed with either PEO or dextran. The virial coefficients obtained in a simultaneous fit involving fitting the critical points of multiple phase diagrams are used to calculate the full original individual phase diagrams. Generally, there is good agreement between such a calculated phase diagram and the original experimental phase diagrams.

1. Introduction

Phase separation is a ubiquitous phenomenon in foods (Tolstoguzov, 1991; Esquena, 2016; Semenova, 2018). Surprisingly little effort has been put into integrating the wealth of experimental data on phase separation in the literature to make practical predictions for phase separation of such mixtures. Practical predictions here refer to forecasts that may not achieve the highest level of accuracy, but are sufficiently precise to guide a researcher or product developer in evaluating the phase behavior of a large number of potential biopolymer combinations. For such an evaluation it is desirable if the assessment requires only a few input parameters from a database.

The present paper aims to develop a general framework to generate such a database for second virial coefficients. The approach is using the Edmond-Ogston model that is based on a virial expansion of the Helmholtz free energy up to second order in concentration (Edmond & Ogston, 1968). On the one hand the advantage of this model is that it based on a systematic expansion of the Helmholtz free energy, while on the other hand it is truncated to include only the minimum number of terms necessary to describe phase separation in binary polymer mixtures. This approach is suitable to describe segregative phase behavior, but ignores some phenomena that are known to affect phase behavior in subtle ways, like polydispersity of the components (Edelman, van der Linden, & Tromp, 2003; Sturtewagen & van der Linden, 2021). As such, it leads to a semi-quantitative prediction of phase behavior of ternary mixtures (two polymers and a solvent), whilst needing only three parameters to do so. This opens the opportunity to create a database of second virial coefficients that allows semi-quantitatively predictions of phase diagrams without the experimental burden of determining the full phase diagrams. Recent progress (Dewi et al., 2020; Bot et al., 2021a, 2021b) facilitates such an analysis, since it provided the necessary insights in the Edmond-Ogston model (analytical expressions for the

Abbreviations: PEO, polyethylene oxide; PEG, polyethylene glycol; BSA, bovine serum albumin.

* Corresponding author.
E-mail address: paul.venema@wur.nl (P. Venema).

https://doi.org/10.1016/j.foodhyd.2021.107473
Received 22 October 2021; Received in revised form 28 November 2021; Accepted 27 December 2021
Available online 29 December 2021

critical point; how multiple virial coefficient combinations give rise to the same critical point).

The approach is illustrated for PEO + dextran mixtures and compared to the second virial coefficients as obtained by membrane osmometry. The choice for the polyethylene oxide/polyethylene glycol - dextran mixtures was made because these mixtures show a clear macroscopic phase separation, and their phase behavior is well-studied in a relatively large number of independent publications. Finally, the approach is also applied to a number of mixtures containing agarose, bovine serum albumin (BSA) or gelatin, mixed with either PEO or dextran.

The virial coefficients obtained in a simultaneous fit of the critical points multiple phase diagrams are used to calculate the full original individual phase diagrams. There is generally good agreement between such a calculated phase diagram and the original experimental phase diagrams.

2. Theory

The parameters of the Edmond-Ogston model (Edmond & Ogston, 1968) are the three second-order virial coefficients (B_{11}, B_{12}, B_{22}). If the biopolymers are modelled as hard spheres with a radius a_i, the second virial coefficients for pure components are proportional to their volume:

$$B_{ii} = \frac{16\pi N_A}{3} a_i{}^3 \tag{1}$$

where N_A is Avogadro's number ($6.02{\cdot}10^{23}$ mol^{-1}). More generally, the second virial coefficient B_{ij} ($m^3 mol^{-1}$) is defined by (McMillan & Mayer, 1945)

$$B_{ij} = 2\pi N_A \int_0^\infty \left(1 - e^{-\frac{w_{ij}(r)}{k_B T}}\right) r^2 dr \tag{2}$$

where $w_{ij}(r)$ is the potential of mean (isotropic) force as a function of the distance r between segments of polymer i and polymer j and k_B is Boltzmann's constant ($1.38{\cdot}10^{-23}$ J/K). Additionally, a relation between the second virial coefficient B_{ii} and the molecular mass $M_{n,i}$ for component i was proposed as (Doi & Edwards, 1986):

$$B_{ii} = k M_{n,i}^{2-b} \tag{3}$$

where b and k are constants. The value for b is reported to be between 0.2 and 0.25 for polymers in a good solvent.

The Edmond-Ogston model relates the second virial coefficients to the Helmholtz free energy as

$$F = RT\left[n_1 \ln\left(\frac{n_1}{V}\right) + n_2 \ln\left(\frac{n_2}{V}\right) + \frac{n_1^2 B_{11}}{V} + \frac{2 n_1 n_2 B_{12}}{V} + \frac{n_2^2 B_{22}}{V}\right] \tag{4}$$

with $T(K)$ the absolute temperature, R ($J/(K{\cdot}mol)$) the gas constant, $V(m^3)$ the total volume of the system, $n_i(mol)$ the number of moles, $B_{ii}(m^3/mol)$ the second virial coefficient of biopolymer i ($i = 1,2$) and B_{12} the second cross virial coefficient for biopolymers 1 and 2. Eq. (4) is the governing equation that allows one to predict the compositions of the co-existing phases where the chemical potential for each component and the osmotic pressure is the same in each phase. One of the main results of previous work (Ersch et al., 2016; Dewi et al., 2020; Dewi et al., 2021; Bot et al., 2021a, 2021b) is that the (infinite) set of second virial coefficients (B_{11}, B_{12}, B_{22}) that give rise to the same critical point ($c_{1,c}, c_{2,c}$) can be written as a line in 'B-space':

$$\begin{pmatrix} B_{11} \\ B_{12} \\ B_{22} \end{pmatrix} = \begin{pmatrix} -\frac{1}{2c_{1,c}} \\ 0 \\ -\frac{1}{2c_{2,c}} \end{pmatrix} + \lambda \begin{pmatrix} \left(\frac{c_{2,c}}{c_{1,c}}\right)^{\frac{2}{3}} \\ 1 \\ \left(\frac{c_{1,c}}{c_{2,c}}\right)^{\frac{2}{3}} \end{pmatrix} \tag{5}$$

Here λ is a real number, where $\lambda > 1/\left(2\left(c_{1,c}{}^{\frac{2}{3}} c_{2,c}{}^{\frac{1}{3}} + c_{1,c}{}^{\frac{1}{3}} c_{2,c}{}^{\frac{2}{3}}\right)\right)$ in order to satisfy the phase separation criterion ${B_{12}}^2/(B_{11}B_{22}) > 1$ (i.e. B_{12} exceeds the geometric mean of B_{11} and B_{22}). Concentrations $c_i = n_i/V$ are expressed in (mol/m^3), where the volume is that of the solution.

Note that eq. (5) indicates that the two coordinates for the critical point ($c_{1,c}$, $c_{2,c}$) are insufficient to determine all three second virial coefficients. In this paper an approach is proposed that circumvents this issue. This approach is based on the observation that for mixtures with common components, the number of second virial coefficients grows slower than the number of critical point coordinates. For example, in a study of the critical points of binary mixtures of the three components A, B and C, six critical point coordinates can be identified as ($c_{1,c}(AB), c_{2,c}(AB), c_{1,c}(AC), c_{2,c}(AC), c_{1,c}(BC), c_{2,c}(BC)$). Also, six second virial coefficients are needed to characterize these systems (B_{AA}, $B_{BB}, B_{CC}, B_{AB}, B_{AC}, B_{BC}$). This means that in this case sufficient information is available to extract all six second virial coefficients from the six critical point coordinates (cf. Fig. 1). In general, from $n \geq 2$ components, and considering all possible binary combinations between those components, $n(n-1)/2$ different mixtures can be composed. These mixtures are described by $n + n(n-1)/2 = n(n+1)/2$ second virial coefficients and $n(n-1)$ critical point coordinates. Note that every mixture provides two critical point coordinates. The number of available equations given by the critical point coordinates exceeds the number of the unknown second virial coefficients by $n(n-3)/2$. At $n = 2$, there is one equation short and indeed it is found that $n(n-3)/2 = -1$. At $n = 3$, one finds $n(n-3)/2 = 0$. For $n = 4$, one finds $n(n-3)/2 = 2$ critical point coordinates too many and it is sufficient to determine the critical point coordinates from 5 of the 6 possible mixtures. In general, one has to measure $n(n+1)/2$ critical point coordinates from $n(n+1)/4$ mixtures to determine $n(n+1)/2$ second virial coefficients. (Note that $n(n+1)/4$ can be an odd number, in case we only need one of the critical point coordinates in one of the mixtures). If the determination of the critical points would be exact, any sub-set of the $n(n+1)/2$ critical point coordinates of the total set of $n(n-1)$ critical point coordinates of would give the same result.

Experimentally, the critical points are determined with limited accuracy and all possible subsets can be used to determine the second virial coefficients from which the error in the virial coefficients can be derived. Such an analysis can be performed in several ways. There is typically not a unique solution for the second virial coefficients that satisfies all critical point coordinates exactly (since the experimental critical point coordinate is not determined exactly due to experimental errors) and optimization techniques should be used. In the analysis below the choice was made to minimize the error in terms of the critical point coordinates, an approach that became much more doable by the recent derivation of analytic expressions for these coordinates.

2.1. Analysis of literature data

Phase diagrams of binary mixtures of dextran and polyethylene oxide/polyethylene glycol (PEO or PEG) were obtained from the literature (Albertsson, 1986; Edmond & Ogston, 1968; Diamond and Hsu, 1989a; Diamond and Hsu, 1989b; Zaslavsky et al., 1989; Forciniti et al., 1991; Connemann et al., 1991; Furuya et al., 1995; Ghosh et al., 2004; Edelman, van der Linden, & Tromp, 2003; Dewi et al., 2020). The names PEO and PEG are chemically synonymous, where PEG refers to polymers with a molecular mass below 20000 g/mol, while PEO refers to molecular masses above 20000 g/mol. Additional diagrams for mixtures

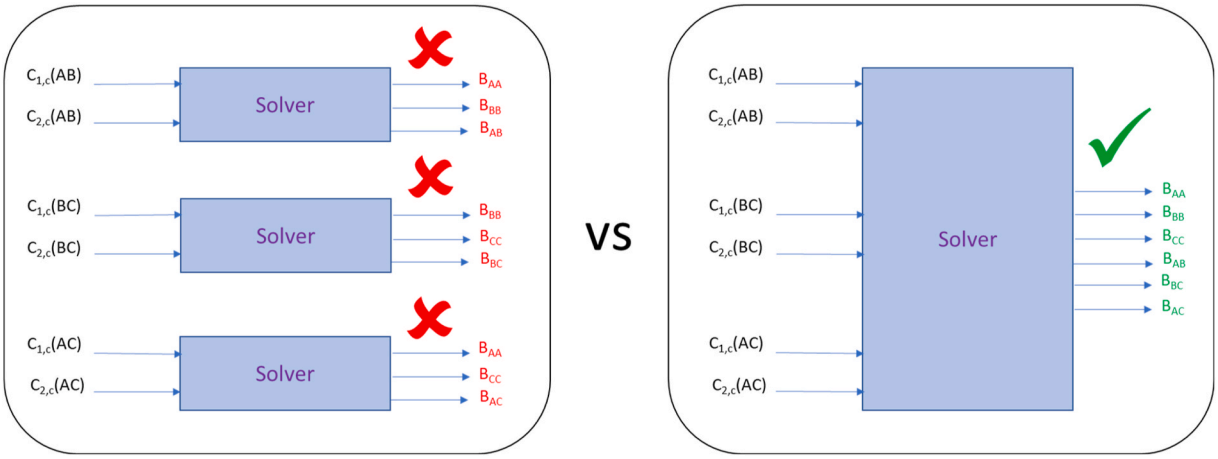

Fig. 1. Schematic illustration of the fitting procedure for mixtures of three polymers A, B and C. The critical point coordinates of each mixture are indicated by $c_{1,c}$ and $c_{2,c}$. The virial coefficients are indicated by the different B's. Left hand side: it is impossible to obtain the virial coefficients if each mixture is fitted individually; Right hand side: a simultaneous fit allows the extraction of all virial coefficients, provided there are at least three mixtures containing shared polymers.

containing agarose, BSA or gelatin, mixed with either PEO or dextran were obtained as well (Edmond & Ogston, 1968; Medin & Janson, 1993; Edelman, Tromp, & van der Linden, 2003; Lee et al., 2020). In total 83 mixtures were analyzed to obtain 109 virial coefficients. Tie-lines and critical point coordinates were extracted using an application that allows for the digitizing graphs. Here the WebPlotDigitizer application (Rohatgi, 2021) was used. In cases where the critical point was not indicated in the plot, its position was estimated using the midpoints of the tie-lines. The initial estimate for the second virial coefficients (B_{11}, B_{12}, B_{22}) was used to calculate S_c, according to (Bot et al., 2021a):

$$S_c = \left(\frac{3\frac{B_{11}}{B_{12}}}{2\sqrt{\left(1+3\frac{B_{11}}{B_{12}}\right)}\cos(\theta) - 1} \right)^2 \tag{6}$$

where:

$$\theta = \frac{1}{3}\cos^{-1}\left(\frac{1}{2} \cdot \frac{27\left(\frac{B_{11}}{B_{12}}\right)^2 \frac{B_{22}}{B_{12}} + 1 - 3\left(1+3\frac{B_{11}}{B_{12}}\right)}{\sqrt{\left(1+3\frac{B_{11}}{B_{12}}\right)^3}} \right) \tag{7}$$

where $-S_c$ corresponds to the slope of the binodal (and spinodal) in the critical point. Next the critical point was estimated by (Bot et al., 2021a):

$$c_{1,c,estimated} = \frac{1}{2(B_{12}S_c - B_{11})} \tag{8}$$

$$c_{2,c,estimated} = \frac{1}{2\left(\frac{B_{12}}{S_c} - B_{22}\right)} \tag{9}$$

(To identify potential numerical errors in evaluating the unwieldy expression for S_c, it is convenient to use the relation $S_c = (c_{2,c,estimated}/c_{1,c,estimated})^{2/3}$ as a consistency check for the result (Bot et al., 2021b)). The sum σ

$$\sigma = \sum_{all\ mixtures} \left\{ \left(\frac{c_{1,c} - c_{1,c,estimated}}{c_{1,c}} \right)^2 + \left(\frac{c_{2,c} - c_{2,c,estimated}}{c_{2,c}} \right)^2 \right\} \tag{10}$$

was minimized, while varying the second virial coefficients as input. This fitting procedure was performed simultaneously for all mixtures, keeping shared second virial coefficients for different mixtures the same and under the assumption that the pure virial coefficients were temperature-independent. Molecular masses were aggregated in twelve bins per decade, having the same width on a logarithmic molecular mass scale. For the stability of the fitting procedure, it was also found useful not to fit B_{12} directly, but rather fit the positive constant δ in $B_{12} = (1+\varepsilon)\sqrt{B_{11}B_{22}} + \delta$ with ε a very small number (typically order (10^{-10})). The first term ensures that the phase separation criterion $\frac{{B_{12}}^2}{B_{11}B_{22}} > 1$ is satisfied, and the positive value for δ ensures that this is also the case for the combination of the first and second term.

Note that the experimental results in the literature were obtained using various experimental protocols and solvent conditions, implicating that the data may not be fully comparable. As the purpose of this paper is mainly to demonstrate the approach of using data analysis, the additional scatter in the result is considered acceptable.

3. Materials and experimental methods

3.1. Materials

Dextran (from Leuconostoc spp.) with the following average molecular masses were used: 40 kDa (D40), 100 kDa (D100), 500 kDa (D500) and 2000 kDa (D2000). Polyethylene oxide (PEO) with two different average molecular masses were used: 35 kDa (PEO35) and 100 kDa (PEO100). MOPS buffer (3-(N-morpholino) propanesulfonic acid) (M1254) was purchased from Sigma-Aldrich. Distilled water (conductivity: 0.055 μS/cm) was used to prepare the solutions.

3.2. Experimental methods

3.2.1. Sample preparation

A 20 mM MOPS buffer was prepared by dissolving MOPS powder in water. By using 1 M NaOH, the pH was adjusted to 6.8. The MOPS buffer was filtered using a 0.22 μm membrane filter (Schleicher & Schuell Bioscience GmbH, Dassel, Germany) and degassed using a vacuum pump for approximately 3 min (Vacuubrand® GmbH, Wertheim, Germany). The MOPS buffer was stored at 4 °C until further use. Stock solutions of PEO and dextran were prepared by dissolving their powders in MOPS buffer. The solutions were continuously stirred (500 rpm) at room temperature, until they were fully dissolved after approximately 1 h. The pH was checked and, if necessary, adjusted using 1 M NaOH or 1M HCl to pH 6.8. All solutions were prepared on a mass base.

3.2.2. Construction of the phase diagram

The phase diagrams of the following PEO-dextran mixtures were determined at 20 °C: (1) PEO35-D40, (2) PEO35-D500, (3) PEO35-

D2000, (4) PEO100-D40, (5) PEO100-D100, (6) PEO100-D500 and (7) PEO100-D2000. The initial solutions of PEO and dextran were diluted with MOPS buffer to obtain samples along dilution lines consisting of at least ten different concentrations. The samples were equilibrated for 24 h before analysis. By adding the dye Brilliant Blue, the phase separation could be clearly identified by the presence of a sharp interface. It was confirmed that the phase volumes were not influenced by the addition of the dye. The critical point is located on the dilution line for which the phase volumes $V^I/V^{II} \rightarrow 1$ on approaching the binodal (Dewi et al., 2020).

3.2.3. Osmotic pressure measurements

For a mixture of two polymers, the osmotic pressure can be written in the Edmond-Ogston model as:

$$\Pi = RT\left(c_1 + c_2 + B_{11}c_1^2 + 2B_{12}c_1c_2 + B_{22}c_2^2\right) \tag{11}$$

where $\Pi(Pa)$ is the osmotic pressure, $c_1(\mathrm{mol}/m^3)$ and $c_2(\mathrm{mol}/m^3)$ are the molar concentrations of polymers 1 and 2, B_{11} and B_{22} are the second virial coefficients of polymers 1 and 2, and B_{12} is the second cross virial coefficient between polymers 1 and 2. This series can be expressed in terms of mass concentration ($\mathrm{kg/m^3}$), as:

$$\Pi = RT\left(\frac{w_1c_w}{\overline{M}_{n,1}} + \frac{w_2c_w}{\overline{M}_{n,2}} + \frac{B_{11}w_1^2c_w^2}{\overline{M}_{n,1}^2} + \frac{B_{22}w_2^2c_w^2}{\overline{M}_{n,2}^2} + \frac{2B_{12}w_1w_2c_w^2}{\overline{M}_{n,1}\overline{M}_{n,2}}\right) \tag{12}$$

where $\overline{M}_{n,1}$ and $\overline{M}_{n,2}$ are the number average molecular masses of polymers 1 and 2 and w_1 and w_2 are the mass fractions of polymers 1 and 2 defined by $w_1 = m_1/(m_1+m_2)$ and $w_2 = m_2/(m_1+m_2)$ where m_1 and m_2 are the masses of polymers 1 and 2. The total mass concentration $c_w = c_{w,1} + c_{w,2}$ where index 1 and 2 refer to polymer 1 and 2.

The osmotic pressures were determined using a membrane osmometer (type 090, Gonotec, GmbH, Germany). Measurements were performed at 20 °C using a 10 kDa cellulose triacetate two-layer membrane. MOPS buffer (15 mM, pH 7.5) was used as a reference solution. The osmometer was left to equilibrate before each measurement for at least 1 h to obtain a stable baseline. The samples were injected from low to high polymer concentration. After injection, equilibrium pressure was typically obtained within 1–10 min. The osmotic pressures of polymers are experimentally measured according to:

$$\Pi = \mathrm{RT}\left(\frac{c_w}{\overline{M}_n} + \overline{A}_2c_w^2\right) \tag{13}$$

where $\overline{M}_n$ is the apparent number average molecular mass and $\overline{A}_2$ is the apparent second virial coefficient. By plotting the reduced osmotic pressures $\Pi' = \Pi/(RTc_w)$ versus the mass concentrations c_w, the inverse of the mass average molecular mass $1/\overline{M}_n$ can be obtained from the intercept, while the virial coefficients $\overline{A}_2$ can be obtained from the slope, when $c_w \rightarrow 0$. Comparing eqs. (12) and (13) and assuming no aggregation takes place, one finds:

$$\frac{1}{\overline{M}_n} = \frac{1}{\overline{M}_{n,2}} + \left(\frac{1}{\overline{M}_{n,1}} - \frac{1}{\overline{M}_{n,2}}\right)w_1 \tag{14}$$

$$\overline{A}_2 = \frac{B_{22}}{\overline{M}_{n,2}^2} + 2\left(\frac{B_{12}}{\overline{M}_{n,1}\overline{M}_{n,2}} - \frac{B_{22}}{\overline{M}_{n,2}^2}\right)w_1 + \left(\frac{B_{22}}{\overline{M}_{n,2}^2} - \frac{2B_{12}}{\overline{M}_{n,1}\overline{M}_{n,2}} + \frac{B_{11}}{\overline{M}_{n,1}^2}\right)w_1^2 \tag{15}$$

By plotting eqs. (14) and (15) as a function of w_1 the virial coefficients and molecular masses can be obtained. The concentration should be expressed in mass per volume. To convert the concentrations, density measurements were performed using a densiometer (DMA 5000, Anton Paar GmbH, Graz, Austria) at 20 °C. The density of the polymer mixtures, $\rho_{mixture}$, were calculated using $\rho_{mixture} = (V_1\rho_1 + V_2\rho_2)/\ V_{mixture}$ and $V_{mixture} = V_1 + V_2$ where ρ_1 is the density of polymer 1, ρ_2 is the density of polymer 2, V_1 is the volume of the polymer 1 solution and V_2 is the volume of the polymer 2 solution. Since the membrane osmometry measurements were limited to the pure components, the above equations simplify to $1/\overline{M}_n = 1/\overline{M}_{n,i}$ and $\overline{A}_2 = B_{ii}/\overline{M}_{n,i}^2$ for $i = 1,2$.

4. Results

4.1. Second virial coefficients extracted from phase diagrams

Virial coefficients for the PEO/PEG + dextran mixtures were obtained from the critical points in the phase diagrams obtained from the literature. It should be noted that this extraction is feasible as a consequence of the recently derived explicit expressions for the critical point, eqs (8) and (9) (Dewi et al., 2020; Bot et al., 2021a). The result is shown in Table 1, which contains the number-averaged molecular weight for both components, the experimental critical point coordinates, the virial coefficients, and the temperature. A second set of virial coefficients was obtained for mixtures containing agarose, BSA or gelatin, mixed with either PEO or dextran. The results are listed in Table 2.

From the fitted virial coefficients in Tables 1 and 2, it is possible to calculate the critical point coordinates and compare these to the values that were obtained experimentally using eqs (6)–(9). The frequency distribution of the ratio Γ of the critical point coordinates as predicted by the second virial coefficients and the experimentally determined critical point coordinates is shown in Fig. 2. The distribution peaks at unity, but has shallow tail towards both sides. In 79% of the cases the predicted value for the critical points coordinates fall within ±10% of their experimental value, and 93% of the cases within ±20% of their experimental value. This is a quite satisfactory result, given the fact that the analysis involved a step in which the published plots were digitized, that critical points were estimated from the tie-line data, and that the experimental data consisted of data obtained in experiments that were not harmonized in terms of protocol.

It is concluded that this method is accurate enough to extract the parameters that predict the primary trends caused by molecular weight, though our analysis excluded an assessment of more subtle effects like temperature or polydispersity.

4.2. Second virial coefficients obtained via membrane osmometry

In order to validate the extraction of virial coefficients from the phase diagram, a limited number of virial coefficients were determined via membrane osmometry as an independent validation of the fitting procedure. In addition, values obtained by Vink (1971) using the same technique are also included in this validation.

The osmotic pressures were measured at 20 °C for two different molecular masses of PEO: PEO35 and PEO100 and for four different molecular masses of dextran: D40, D100, D500 and D2000. The phase behaviour of PEO35-D100 has been determined before (cf. Dewi et al. (2020)) at 20 °C. The typical concentrations used in these measurements ranged from 0.1 to 2% (w/w). Fig. 3 shows the reduced osmotic pressure $\Pi' = \frac{\Pi}{RTc_w}$ versus the mass concentration c_w of PEO ($c_{w,1}$) and dextran ($c_{w,2}$) for different molecular masses. From Fig. 3, the number average molecular mass $\overline{M}_{n,i}$ and the second virial coefficients B_{11} (PEO) and B_{22} (dextran) were determined (cf. Table 3). Table 3 also contains values reported by Vink (1971).

Table 3 summarises the second virial coefficients as determined experimentally by membrane osmometry. Increasing the molecular mass of dextran, at a fixed molecular mass of PEO, the phase separation takes place at lower total polymer concentration. Similarly, increasing the molecular mass of PEO, at a fixed molecular mass of dextran, the phase separation also takes place at lower total polymer concentration. This is in line with previously reported results on a similar mixture at lower molecular masses (Forciniti et al., 1991).

Table 1
Number averaged molecular weights $M_{n,i}$, coordinates of the critical point $c_{i,c}$, fitted virial coefficients B_{ij} of the PEG/PEO + dextran mixtures as used in this analysis, and temperature T at which the experiment was performed.

component1/component2	$M_{n,PEG}$	$M_{n,dextran}$	$c_{PEG,c}$	$c_{dex,c}$	$B_{PEG,PEG}$	$B_{dextran,\ dextran}$	$B_{PEG,\ dextran}$	T	Reference
	g/mol	g/mol	mol/m^3	mol/m^3	m^3/mol	m^3/mol	m^3/mol	°C	
PEG 4000/DEX T40	2900	18800	22.7	5.02	0.00503	0.114	0.0761	20	Furuya et al. (1995)
PEG 4000/DEX T70	2900	37900	21.6	1.98	0.00503	0.400	0.140	20	Furuya et al. (1995)
PEG 4000/DEX 140	2900	35600	21.0	1.94	0.00503	0.400	0.140	20	Furuya et al. (1995)
PEG 4000/DEX T500(a)	2900	191000	20.3	0.304	0.00503	5.86	0.474	20	Furuya et al. (1995)
PEG 6000/DEX T500(b)	8500	170300	3.76	0.276	0.0652	5.86	1.23	20	Furuya et al. (1995)
PEG 3400/DEX T40	3400	24200	16.4	3.51	0.00503	0.126	0.0977	4	Diamond and Hsu (1989a)
PEG 3400/DEX T70	3400	38400	15.0	1.80	0.00503	0.354	0.156	4	Diamond and Hsu (1989a)
PEG 3400/DEX T500	3400	234200	14.1	0.188	0.00503	9.70	0.689	4	Diamond and Hsu (1989a)
PEG 8000/DEX T40	8000	24200	4.62	3.10	0.0652	0.126	0.223	4	Diamond and Hsu (1989a)
PEG 8000/DEX T70	8000	38400	3.92	1.51	0.0652	0.354	0.363	4	Diamond and Hsu (1989a)
PEG 8000/DEX T500	8000	234200	3.39	0.156	0.0652	9.70	1.66	4	Diamond and Hsu (1989a)
PEG 20000/DEX T40	20000	24200	1.96	1.68	0.0709	0.126	0.373	4	Diamond and Hsu (1989a)
PEG 20000/DEX T70	20000	38400	1.80	0.886	0.0709	0.354	0.566	4	Diamond and Hsu (1989a)
PEG 20000/DEX T500	20000	234200	1.30	0.0790	0.0709	9.70	2.74	4	Diamond and Hsu (1989a)
PEG 20000/DEX T40	20000	24200	2.07	2.03	0.0709	0.148	0.360	22	Diamond and Hsu (1989b)
PEG 20000/DEX T70	20000	38400	2.03	0.794	0.0709	0.400	0.573	22	Diamond and Hsu (1989b)
PEG 20000/DEX T500	20000	234200	1.51	0.0697	0.0709	12.4	2.87	22	Diamond and Hsu (1989b)
PEG 8000/DEX T40	8000	24200	5.09	3.05	0.0652	0.148	0.221	22	Diamond and Hsu (1989b)
PEG 8000/DEX T70	8000	38400	4.86	1.65	0.0652	0.400	0.336	22	Diamond and Hsu (1989b)
PEG 8000/DEX T500	8000	234200	4.01	0.139	0.0652	12.4	1.70	22	Diamond and Hsu (1989b)
PEG 3400/DEX T40	3400	24200	19.1	3.69	0.00503	0.148	0.0942	22	Diamond and Hsu (1989b)
PEG 3400/DEX T70	3400	38400	18.4	2.01	0.00503	0.400	0.140	22	Diamond and Hsu (1989b)
PEG 3400/DEX T500	3400	234200	16.9	0.191	0.00503	12.4	0.717	22	Diamond and Hsu (1989b)
PEG 4000/DEX 19	3810	27705	13.5	2.98	0.005	0.148	0.115	40	Forciniti et al. (1991)
PEG 4000/DEX 17	3810	13239	16.4	7.56	0.005	0.0384	0.0611	40	Forciniti et al. (1991)
PEG 4000/DEX 37	3810	52066	11.5	1.71	0.005	0.715	0.226	40	Forciniti et al. (1991)
PEG 4000/DEX 48	3810	88252	10.8	0.669	0.005	1.24	0.32	40	Forciniti et al. (1991)
PEG 4000/DEX 17	3810	13239	17.8	7.70	0.005	0.0384	0.0585	25	Forciniti et al. (1991)
PEG 6000/DEX 17	5318	13239	10.8	7.25	0.0125	0.0384	0.0797	25	Forciniti et al. (1991)
PEG 10000/DEX 17	10216	13239	4.04	6.54	0.105	0.0384	0.162	25	Forciniti et al. (1991)
PEG 20000/DEX 17	19081	13239	1.86	5.84	0.364	0.0384	0.281	25	Forciniti et al. (1991)
PEG 4000/DEX 48	3810	88252	11.0	0.689	0.005	1.24	0.315	25	Forciniti et al. (1991)
PEG 6000/DEX 48	5318	88252	7.33	0.578	0.0125	1.24	0.415	25	Forciniti et al. (1991)
PEG 10000/DEX 48	10216	88252	2.35	0.623	0.105	1.24	0.805	25	Forciniti et al. (1991)
PEG 20000/DEX 48	19081	88252	1.05	0.601	0.364	1.24	1.32	25	Forciniti et al. (1991)
PEG 6000/DEX 19,7	8000	19700	6.0	4.3	0.0652	0.111	0.183	28	Edmond and Ogston (1968)
PEG 6000/DEX 27.2	8000	27200	6.5	3.0	0.0652	0.148	0.221	28	Edmond and Ogston (1968)
PEG 6000/DEX 37.5	8000	37500	5.3	1.9	0.0652	0.400	0.336	28	Edmond and Ogston (1968)
PEG 6000/DEX 52.8	8000	52800	5.1	1.1	0.0652	0.715	0.434	28	Edmond and Ogston (1968)
PEG 20000/DEX 19.7	19400	19700	1.7	3.6	0.364	0.111	0.407	28	Edmond and Ogston (1968)
PEG 20000/DEX 27.2	19400	27200	1.6	2.2	0.364	0.148	0.503	28	Edmond and Ogston (1968)
PEG 20000/DEX 37.5	19400	37500	1.4	1.6	0.364	0.400	0.719	28	Edmond and Ogston (1968)
PEG 20000/DEX 52.8	19400	52800	1.4	0.99	0.364	0.715	0.932	28	Edmond and Ogston (1968)
PEG 6000/DEX 70	6000	28700	6.67	2.79	0.0125	0.126	0.165	8	Zaslavsky et al. (1989)
PEG 6000/DEX 70	6000	28700	7.17	2.75	0.0125	0.148	0.166	23	Zaslavsky et al. (1989)
PEG 6000/DEX 70	6000	28700	7.83	2.75	0.0125	0.148	0.158	38	Zaslavsky et al. (1989)
PEG 6000/DEX 70	6000	28700	8.00	2.72	0.0125	0.148	0.158	50	Zaslavsky et al. (1989)
PEG 6000/DEX T40	6000	16000	8.74	3.61	0.0125	0.0879	0.126	30	Ghosh et al. (2004)
PEG 6000/DEX T500	6000	170000	9.3	0.247	0.0125	5.86	0.725	30	Ghosh et al. (2004)
PEG 3000/DEX 500	3140	101000	16.4	0.624	0.00503	2.25	0.328	0	Connemann et al. (1991)
PEG 3000/DEX 500	3140	101000	20.2	0.629	0.00503	2.25	0.301	20	Connemann et al. (1991)
PEG 3000/DEX 500	3140	101000	21.2	0.604	0.00503	2.25	0.298	40	Connemann et al. (1991)
PEG 4000/DEX D17	4000	17000	15.9	3.59	0.00500	0.114	0.0961	20	Albertsson (1986)
PEG 3350/DEX T500	3350	200000	14.6	0.275	0.00503	9.70	0.689	0	Albertsson (1986)
PEG 8000/DEX T500	8000	200000	4.13	0.220	0.0652	12.4	1.70	20	Albertsson (1986)
PEO 35/DEX 40	45210	29250	0.47	2.5	3.68	0.293	1.53	20	This work
PEO 35/DEX 100	45210	61670	0.40	1.1	3.68	0.715	2.42	20	Dewi et al. (2020)
PEO 35/DEX 500	45210	377610	0.32	0.13	3.68	13.8	9.62	20	This work
PEO 35/DEX 2000	45210	871000	0.32	0.060	3.68	50.5	17.5	20	This work
PEO 100/DEX 40	53410	29250	0.40	1.9	3.02	0.293	1.54	20	This work
PEO 100/DEX 100	53410	61670	0.27	0.79	3.02	0.715	2.58	20	This work
PEO 100/DEX 500	53410	377610	0.25	0.090	3.02	13.8	9.87	20	This work
PEO 100/DEX 2000	53410	871000	0.23	0.030	3.02	50.5	18.8	20	This work
PEO 100/DEX 299k	39000	64000	0.436	0.375	1.18	1.51	2.57	50	Edelman, van der Linden, and Tromp (2003)

5. Discussion

5.1. Power-law behaviour for the pure virial coefficients

The relationship between the second virial coefficients of PEO and dextran as a function of the number average molecular mass is shown in Fig. 4 and Fig. 5. Fig. 4 shows the second virial coefficient $B_{dextran,\ dextran}$ as a function of the molecular weight M_n as obtained from Table 1. Despite the differences in experimental protocols in these studies, a consistent picture emerges, where the results closely follow the power law as $B_{dextran,dextran} = kM_{n,dextran}^{2-b}$ where $k = 2.18.10^{-9}$ (m^3/mol), $b = 0.21$ and $M_{n,dextran}$ expressed in (g/mol). Fig. 4 also includes the values

Table 2
Number averaged molecular weights $M_{n,i}$, coordinates of the critical point $c_{i,c}$, fitted virial coefficients B_{ij} of the mixtures of either PEG/PEO or dextran with agarose, bovine serum albumin (BSA) or gelatin as used in this analysis and temperature T at which the experiment was performed. Gelatin B stands for bovine gelatin, gelatin P for porcine gelatin.

component1/component2	$M_{n,1}$	$M_{n,2}$	$c_{1,c}$	$c_{2,c}$	B_{11}	B_{22}	B_{12}	T	Reference
	g/mol	g/mol	mol/m^3	mol/m^3	m^3/mol	m^3/mol	m^3/mol	°C	
PEG 6000/agarose	6000	120000	5.08	0.332	0.0125	2.93	0.701	80	Medin and Janson (1993)
PEG 20000/agarose	20000	120000	0.835	0.202	0.0709	2.93	1.93	80	Medin and Janson (1993)
PEG 35000/agarose	35000	120000	0.354	0.200	1.18	2.93	3.75	80	Medin and Janson (1993)
agarose/dextran X25	120000	25000	0.364	3.22	2.93	0.148	1.17	80	Medin and Janson (1993)
agarose/dextran T40	120000	40000	0.265	1.02	2.93	0.400	2.08	80	Medin and Janson (1993)
agarose/dextran T70	120000	70000	0.283	0.373	2.93	1.51	3.66	80	Medin and Janson (1993)
PEG 6000/BSA	8000	73200	4.63	2.28	0.0652	0.207	0.272	28	Edmond and Ogston (1968)
PEG 20000/BSA	19400	73200	1.39	2.08	0.364	0.207	0.570	28	Edmond and Ogston (1968)
PEG 10000/gelatin (GP)	10000	75000	3.38	1.11	0.105	0.948	0.597	50	Lee et al. (2020)
PEG 10000/gelatin (GB)	10000	50000	3.44	2.65	0.105	0.477	0.426	50	Lee et al. (2020)
PEG 4000/gelatin (GP)	4000	75000	15.1	1.00	0.00500	0.948	0.234	50	Lee et al. (2020)
PEG 4000/gelatin (GB)	4000	50000	16.2	2.89	0.00500	0.477	0.159	50	Lee et al. (2020)
PEG 6000/gelatin (GP)	6000	75000	8.58	1.08	0.0125	0.948	0.318	50	Lee et al. (2020)
PEG 6000/gelatin (GB)	6000	50000	8.27	2.56	0.0125	0.477	0.235	50	Lee et al. (2020)
PEG 2000/gelatin (GP)	2000	75000	46.5	1.19	0.00500	0.948	0.157	50	Lee et al. (2020)
PEG 2000/gelatin (GB)	2000	50000	63.8	1.80	0.00500	0.477	0.116	50	Lee et al. (2020)
PEG 8000/gelatin (GP)	8000	75000	5.33	1.14	0.0652	0.948	0.469	50	Lee et al. (2020)
PEG 8000/gelatin (GB)	8000	50000	8.02	1.34	0.0652	0.477	0.350	50	Lee et al. (2020)
gelatin 170k/DEX 282k	97000	64000	0.335	0.492	2.72	1.51	3.26	50	Edelman, Tromp, and van der Linden (2003)

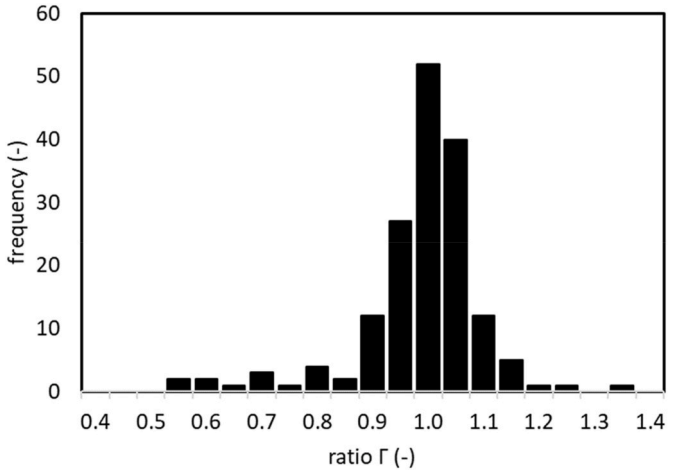

Fig. 2. Accuracy of fit to the critical coordinates for the full dataset, as given by the frequency distribution as a function of the ratio Γ of the critical point coordinates as predicted by the fitted second virial coefficients and the experimentally determined critical point coordinates. A perfectly fitted critical point coordinate is in bin '1.0'. Bin size ±0.025.

for the second virial coefficients as obtained by membrane osmometry (this work, Vink (1971)) The osmometry results agree well with the values obtained by fitting the phase diagrams, even though these are completely different techniques and much bigger differences might have been expected.

A similar result is obtained for the second virial coefficient $B_{PEG,\ PEG}$, as shown in Fig. 5. Again, a power law behavior as $B_{PEG,\ PEG} = kM_{n,PEG}^{2-b}$ is observed, where $k = 7.69.10^{-11}\ (m^3/mol)$, $b = -0.24$ and $M_{n,PEG}$ expressed in *(g/mol)*. Any effect of temperature is small compared to the scatter in the data of the second virial coefficients. Again, the agreement of the virial coefficients as extracted from literature with membrane osmometry (this study, Vink (1971)) is good.

5.2. The cross-virial coefficient and a closure relation

Fundamentally, it is impossible to derive the cross second virial coefficient from the values of the second virial coefficients of the pure components. Nevertheless, it is often possible to guess an approximate value based on a simple mixing rule. Such a simple mixing rule could be inferred from Fig. 6 as:

$$B_{12} = \left(\frac{B_{11}^{1/3} + B_{22}^{1/3}}{2}\right)^3 \tag{16}$$

which is a generalization of the hard sphere mixing rule as discussed earlier (Ersch et al., 2016) and this mixing rule is expected to be applicable to most polymers, assuming most polymers have limited interpenetration. Fig. 6 shows that the above mixing rule eq. (16) for the dextran-PEG mixtures provides a suitable first order approximation for the second cross virial coefficient, in particular at higher values of B_{12} (i.e. values above 1). The deviations for small polymer coils should probably be interpreted as an interface/surface effect, which is significant for small polymer coils but can be ignored for large polymer coils (where the surface to volume ratio is smaller).

The consequences of the mixing rule in eq (16) can be investigated in somewhat more detail. Introducing the ratio $q = B_{11}^{1/3}/B_{22}^{1/3}$, eq (16) can be written in two ways

$$B_{12} = B_{11}\left(\frac{1+\frac{1}{q}}{2}\right)^3 = B_{22}\left(\frac{q+1}{2}\right)^3 \tag{17}$$

In the hard sphere approximation, q would be the ratio of the radii of the spheres. The phase separation criterion can now be written as

$$\frac{B_{12}^2}{B_{11}B_{22}} = \left(\frac{q^{1/2} + q^{-1/2}}{2}\right)^6 > 1 \tag{18}$$

This relation is valid for all q≠1, as was shown for the hard-sphere case by Ersch et al. (2016). In other words, this mixing rule implies that a system behaving according to the mixing rule will phase separate at sufficiently high concentration unless the 'pure' second virial coefficients of both components in the mixture are identical (i.e. $q = 1$) (see Fig. 7(a)).

The critical coordinates are given now by

$$c_{1,c} = \frac{1}{2B_{11}\left(S_c\left(\frac{1+1/q}{2}\right)^3 - 1\right)} \tag{19}$$

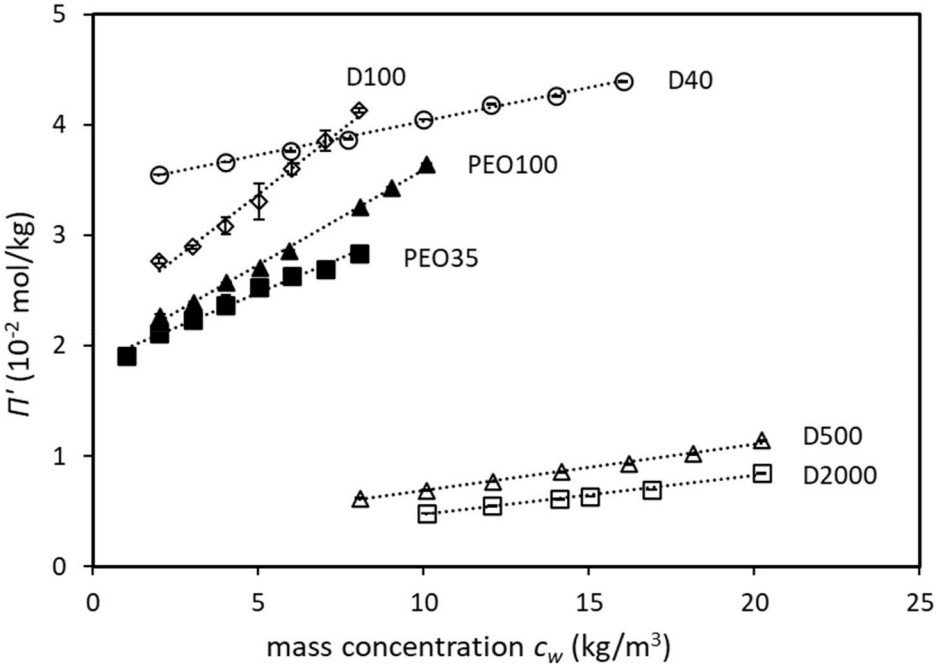

Fig. 3. The reduced osmotic pressure Π' = Π/(RTc$_w$) versus mass concentration c$_w$ of PEO and dextran for different molecular masses at 20 °C: (filled symbols) PEO; (open symbols) dextran. The dashed lines represent the linear fit to the data.

Table 3
The number averaged molecular masses $\overline{M}_n$ and the second virial coefficients B_{11} of PEO and dextran D for different molecular masses at 20 °C as measured via osmotic pressure measurements. Values obtained by Vink (1971) at 25 °C are added as well.

	$\overline{M}_n$ (kg/mol)	B_{11} (m^3/mol)	Reference
PEO35	45.2 ± 0.4	4.74 ± 0.04	Dewi et al. (2020)
PEO100	53.4 ± 0.2	4.91 ± 0.04	This work
D40	29.3 ± 0.1	0.52 ± 0.1	This work
D100	61.7 ± 0.2	1.31 ± 0.03	Dewi et al. (2020)
D500	377 ± 1	60.0 ± 0.3	This work
D2000	871 ± 4	269 ± 3	This work
D1	28.7	0.446	Vink (1971)
D2	374	59.5	Vink (1971)
PEO	43.5	3.66	Vink (1971)

$$c_{2,c} = \frac{1}{2B_{22}\left(\frac{1}{S_c}\left(\frac{q+1}{2}\right)^3 - 1\right)} \tag{20}$$

and eqs (22) and (23) from (Bot et al., 2021a) can be rewritten as

$$S_c = \left(\frac{3\left(\frac{2}{1+\frac{1}{q}}\right)^3}{2\sqrt{\left(1+3\left(\frac{2}{1+\frac{1}{q}}\right)^3\right)\cos(\theta) - 1}}\right)^2 \tag{21}$$

with

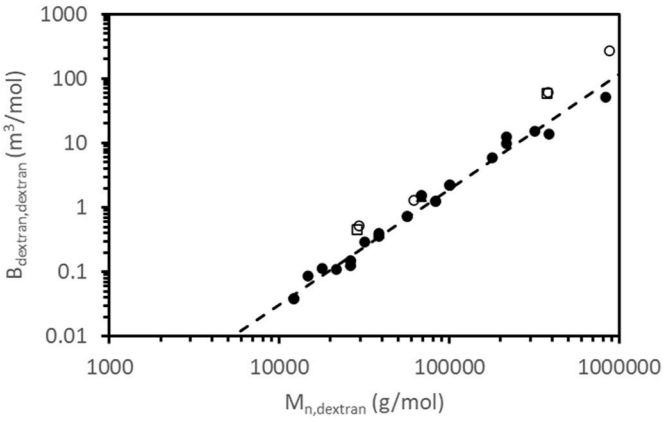

Fig. 4. The dextran-dextran second virial coefficients: (●) as extracted from critical point coordinates obtained from phase diagrams available in the literature; (○) determination by membrane osmometry, this study; (□) determination by membrane osmometry, Vink (1971); (- - -) power law fit to the data points extracted from the literature with slope 1.79 (standard deviation of ±0.04).

$$\theta = \frac{1}{3}cos^{-1}\left(\frac{1}{2}\cdot\frac{27\left(\left(\frac{2}{1+\frac{1}{q}}\right)^3\right)^2\left(\frac{2}{q+1}\right)^3 + 1 - 3\left(1+3\left(\frac{2}{1+\frac{1}{q}}\right)^3\right)}{\sqrt{\left(1+3\left(\frac{2}{1+\frac{1}{q}}\right)^3\right)^3}}\right) \tag{22}$$

Note that for $q = 1$ and S_c close to 1, the critical points will move towards infinity, as expected. Since for hard spheres $\varphi = (B_{11}c_1 + B_{22}c_2)/4$ (Bot et al., 2021a), it is expected that the maximum volume fraction at the critical point is around order (1)

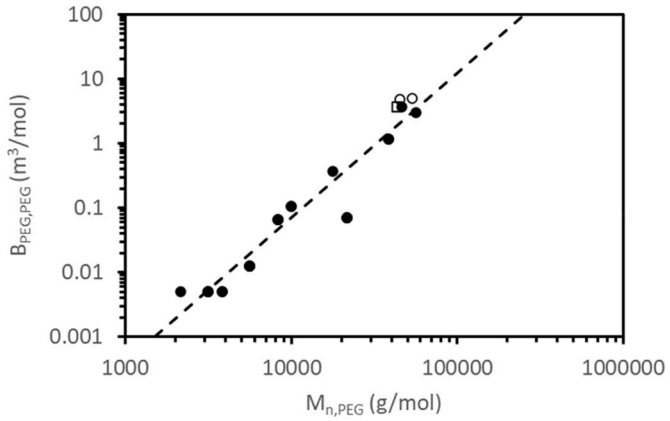

Fig. 5. PEG-PEG second virial coefficients: (●) as extracted from critical point coordinates obtained from phase diagrams available in the literature; (○) determination by membrane osmometry, this study; (□) determination by membrane osmometry, Vink (1971); (- - - -) power law fit to the data points extracted from the literature with slope 2.24 (standard deviation of ±0.12).

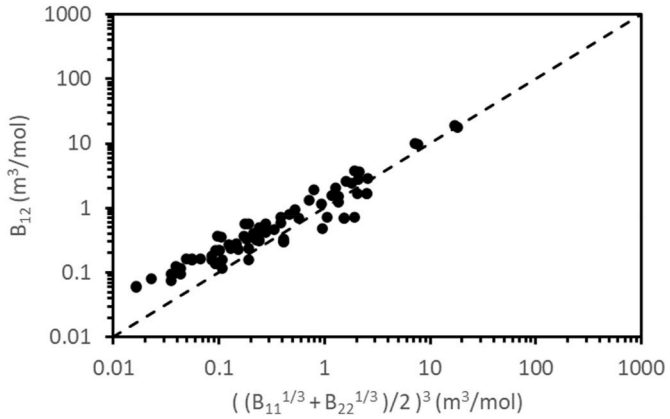

Fig. 6. Prediction for the dextran-PEG cross second virial coefficient B_{12} based on the simple mixing rule in eq (16). The values on the horizontal axis are calculated from the experimental second virial coefficients for the single components as given in Table 1, and the vertical axis shows both the (dots) predicted and (dashed line) estimated (eq (16)) cross-virial coefficients.

$$\frac{B_{11}c_{1,c}+B_{22}c_{2,c}}{4}=\frac{1}{8}\left(\frac{1}{\left(S_c\left(\frac{1+1/q}{2}\right)^3-1\right)}+\frac{1}{\left(\frac{1}{S_c}\left(\frac{q+1}{2}\right)^3-1\right)}\right) \tag{23}$$

So, for a volume fraction of order (1) (and taking order (1) here as being exactly 1 for the sake of this discussion), q needs to exceed 2.2 [see Fig. 7(b)]. This implies that B_{11}/B_{22} needs to be larger than ~10. For dextran, where B depends on molecular weight according to a power law with exponent 1.79, this means that the molecular weight ratio for the two polymers needs to be at least ~4.3 to show phase separation. Practically, the above calculation should be taken as an order of magnitude calculation and not as an exact result.

5.3. Reconstruction of phase diagrams based on extracted second virial coefficients

Below it will be evaluated how well the virial coefficients obtained from a simultaneous fit of the critical points of multiple phase diagrams predict the complete individual phase diagrams in the data set. This is not a trivial check, because also information from all the other phase diagrams is used to extract the virial coefficients for a specific mixture.

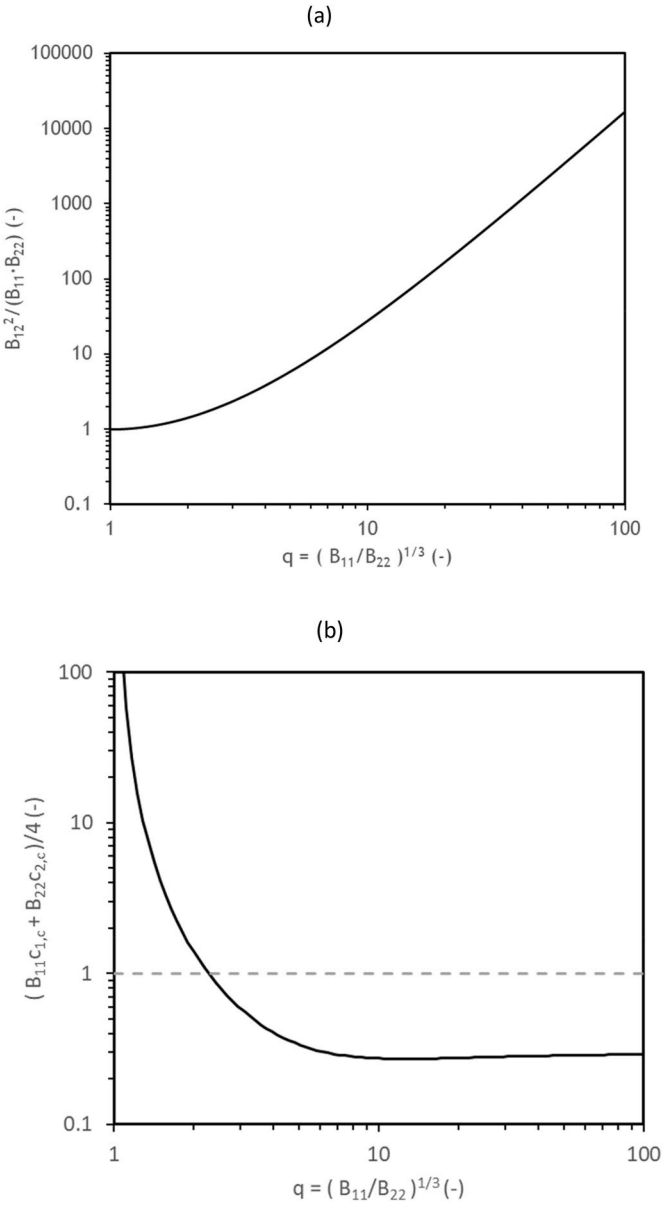

Fig. 7. (a) Phase separation criterion $B_{12}^2/(B_{11}B_{22})$ as a function of the ratio $q = B_{11}^{1/3}/B_{22}^{1/3}$. The function is invariant under the substitution q → 1/q, and is therefore mirror-symmetrical around the q = 1 axis in this plot; (b) Hard spheres equivalent volume fraction for the critical point as a function of the ratio $q = B_{11}^{1/3}/B_{22}^{1/3}$. The function is invariant under the substitution q → 1/q, and is therefore mirror-symmetric around the q = 1 axis in this plot. The dashed line is the maximum packing fraction, assuming this to be of order (1).

Also, it is noted that the virial coefficients are based only on the critical points, and the predictions include all aspects of the phase diagrams (e.g. including a prediction of the tie-lines). Below this approach will be evaluated for PEO/PEG + dextran mixtures, for PEO/PEG + dextran from the literature. Finally, this comparison is also made for mixtures containing either PEO or dextran in combination with other hydrocolloids (agarose, BSA or gelatin). The phase diagrams were calculated using the procedure described in Bot et al. (2021a).

5.3.1. Completing the phase diagram for data obtained using the dilution method

In Fig. 8, two of the reconstructed phase diagrams are shown for PEO and dextran mixtures from Table 1: PEO35 + D40 and PEO35 + D100, respectively. As in previous work (Dewi et al., 2020), the fitted phase

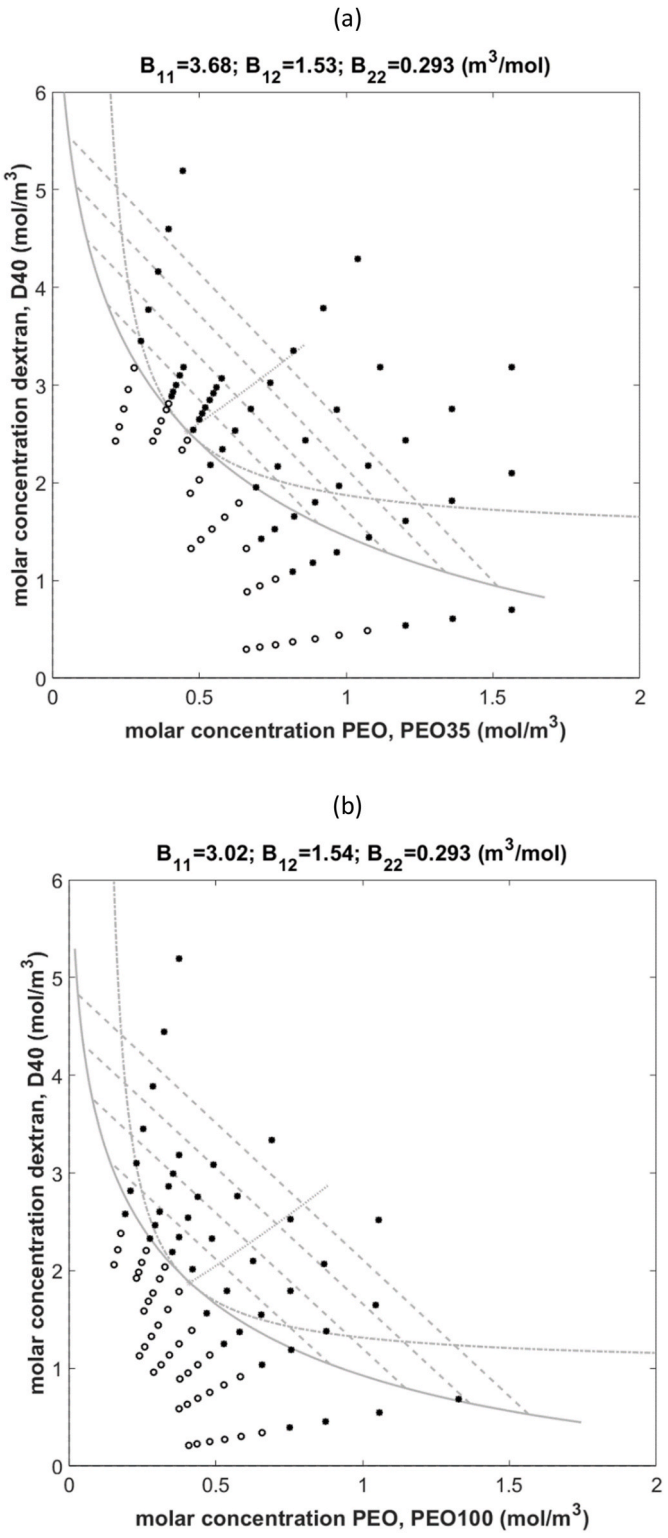

Fig. 8. The phase diagrams at 20 °C for mixtures of (a) PEO35-D40 and (b) PEO100-D40. The open black symbols represent one-phase mixtures, while the closed black symbols represent two-phase mixtures. The critical point for PEO35-D40 is at ($c_{1,c} = 0.47$ mol/m^3, $c_{2,c} = 2.49$ mol/m^3), and for PEO100-D40 at ($c_{1,c} = 0.40$ mol/m^3, $c_{2,c} = 1.90$ mol/m^3). The predicted binodal (solid line, grey), the predicted spinodal (dash-dotted line, grey), midpoints of tie-lines (dotted line), and the predicted tie-lines (dashed line, grey). All the values were calculated using the values for the second virial coefficients from Table 1.

diagram gives a fair representation of the binodal. In the present analysis, consistency with many other phase diagrams is assured simultaneously, resulting in more reliable estimates for the virial coefficients. The agreement is better on the dextran-rich side of the phase diagram, relative to the critical point, as observed previously. On the PEO-rich side of the binodal, the data in Fig. 8(a) and (b) seem to indicate a larger phase separating region than the fit does. In other phase diagrams in the literature, such behaviour is usually not observed, but it should be noticed that the molecular weights of the polymers used in those experiments are usually lower. The difference between calculated and experimental phase diagram could be caused by polydispersity effects of the polymers. Fractionation may occur in polydisperse samples, thereby distorting the phase diagram when the axes are plotted in a way that does not take fractionation in account. The phase separating region moves closer to the axis if one of the phases becomes enriched in high-molecular weight polymers (cf. Sturtewagen et al., 2021). The critical point itself is not affected by polydispersity effects, because fractionation does not occur at the critical point. In addition, there is a potential effect of incomplete phase separation at higher molecular weight, in particular when the viscosity of the continuous phase increases at higher polymer concentrations. Since the method to obtain the data in Fig. 8 does not test the predicted slope of the tie-lines, literature data will be used to compare this aspect of the prediction.

5.3.2. Comparing the phase diagram to PEG/PEO + dextran data found in the literature

The second virial coefficients as obtained from the critical points were used to determine the phase diagrams as predicted by the Edmond-Ogston model. Elements of the phase diagrams like spinodal, binodal, tie-lines and critical point - which follow from the choice of the virial coefficients - were plotted allowing for a comparison to the original experimentally determined phase diagram.

The first example is a diagram in which the critical point coordinates are perfectly matched in the fitting procedure, and for which tie-lines are reported. For this comparison a diagram based on data published by Edmond and Ogston (1968) on PEO6000 and dextran 19.7 is chosen. It can be seen from Fig. 9(a) that the predicted tie-lines, despite not being part of the fit directly, match the experimentally observed tie-lines very well. Also, the experimental binodal matches the predicted binodal well, despite giving rise to a slightly smaller phase separating region. For the next system, a more asymmetric mixture DEXT40 + PEG3400 is chosen (Diamond and Hsu, 1989b). Fig. 9(b) shows that the prediction for the tie-lines is still decent. The binodal is predicted more accurate in the PEG-rich phase than in the dextran-rich phase. However, the predicted phase separation region in the fit is smaller than in the experimental data, and the difference is noticeably bigger than for the previous mixture. The third system, PEG6000 + DEXT40 (Ghosh et al., 2004), is slightly less asymmetric than the previous one, but features a PEG with a higher molecular weight. Fig. 9(c) shows generally good agreement between data and calculation, though the slope of the prediction differs more from the experimental result than in the previous two cases. The fourth system represents the strongly asymmetric mixture DEX500 + PEG3000 (Connemann et al., 1991). Fig. 9(d) shows, again, the binodal is predicted more accurate in the PEG-rich phase than in the dextran-rich phase, and the mismatch between the predicted and experimental phase separating region has increased. There is a bigger mismatch between the predicted and experimentally observed slope of the tie-lines.

It can be concluded that the Edmond-Ogston model can be used to describe the PEG + dextran phase diagrams for a wide range of molecular weights obtained by a number of different authors. The fits do not superimpose exactly, either due to limitations of the Edmond-Ogston model (i.e. the truncation of the virial expansion, not taking into account third and higher order terms in concentration) or due to differences in experimental protocols used for obtaining the experimental data (e.g. determining the binodal by letting an unstable mixture phase separate and determining the composition of the separated phases

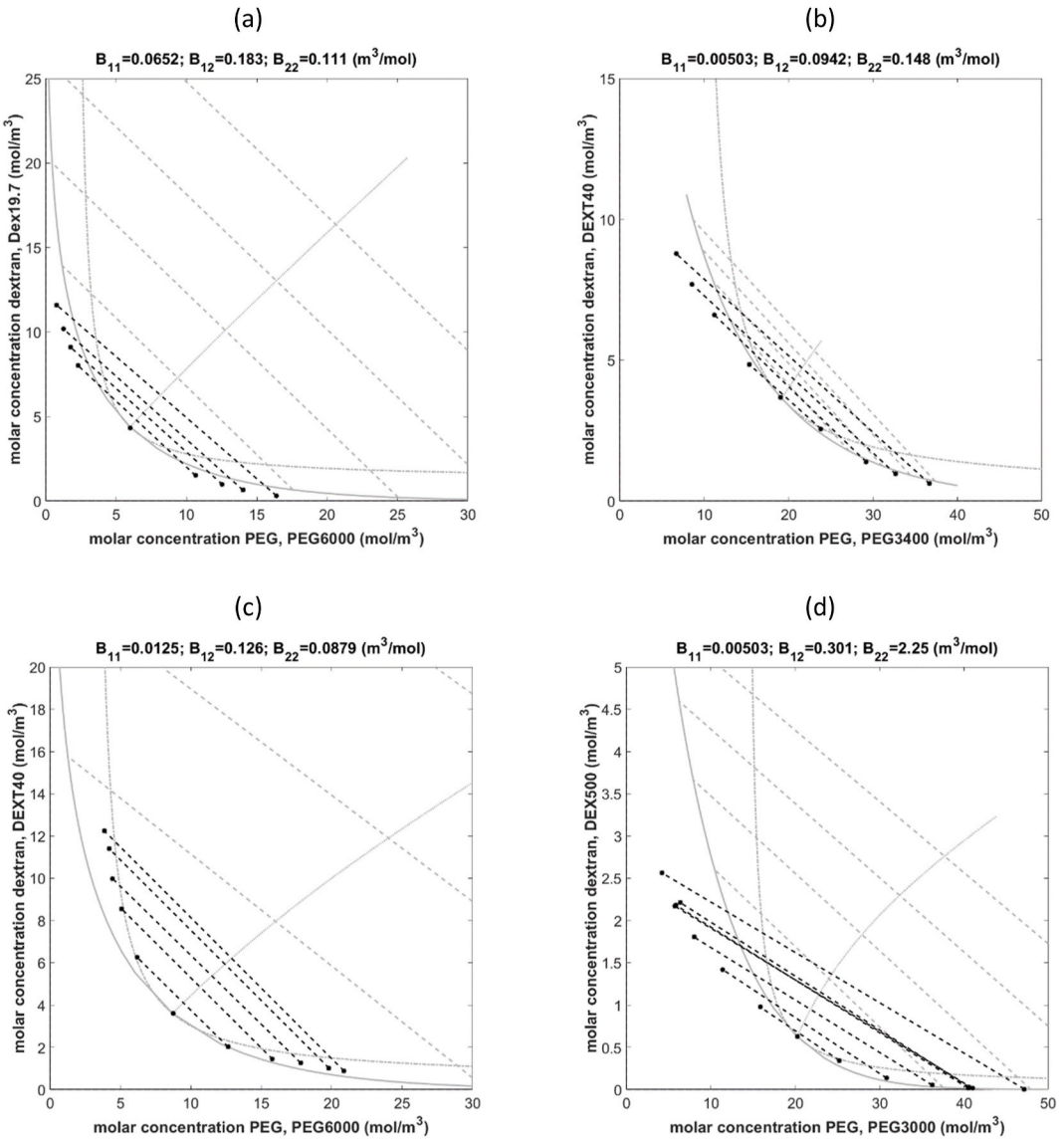

Fig. 9. Phase diagram for (a) PEG6000 + Dex 19.7 at 28 °C by Edmond and Ogston (1968); (b) PEG3400 + DEXT40 at 22 °C by Diamond and Hsu (1989b); (c) PEG6000 + DEXT40 at 30 °C by Ghosh et al. (2004); (d) PEG3000 + DEX500 at 20 °C by Connemann et al. (1991): (black) experimental data; (grey) present fit; (solid line) binodal; (dash-dotted line) spinodal; (dashed line) tie-lines; (dotted line) midpoints of tie-lines; (●) critical point and end-points of experimental tie-lines. For the virial coefficients mentioned in the header, component '1' is plotted along the horizontal axis, whereas component '2' is plotted along the vertical axis.

versus the dilution line method, differences in techniques used to determine the concentration of components in upper and lower phase, methods to handle incomplete phase separation in case that occurs), but overall the overlap is sufficient to make the predictions practically useful.

5.3.3. Comparing the phase diagram to literature data on systems containing one other component than PEG/PEO or dextran

The above approach can be extended to systems containing one other component than either PEG/PEO or dextran, and Fig. 10 displays a number of those examples involving bovine serum albumin (BSA), agarose and gelatin. The mixture PEG8000 + porcine gelatin shown in Fig. 10(a) (Lee et al., 2020) shows a slightly narrower phase separation area in the prediction, and the better fit to the binodal for PEG-rich phases. The slopes of the tie-lines of the fit and experiment match well, and the general appearance of the fit is similar to that of the experimental result. Fig. 10(b) shows the phase diagram of the agarose + DEXX25 mixture (Medin & Janson, 1993). The critical point is relatively far away from the prediction, as is the binodal for agarose-rich samples. The difference in location of the binodal in the agarose-rich region of the phase diagram may point at arrested or incomplete phase separation (micro phase separation). The slopes of the experimental tie-lines vary considerably, and the predicted slopes are with the range. Fig. 10(c) shows a very good match to the gelatin + dextran phase diagram as obtain by Edelman, Tromp, and van der Linden (2003). In this case both the critical point and the tie-lines are very well represented by result of the simultaneous fit of multiple phase diagrams. The PEG20000 + BSA diagram, Fig. 10(d) illustrates that the procedure in this paper uses only the critical point and not the tie-lines of the experimental phase diagram. For this mixture, Edmond and Ogston (1968) only published the critical point and not the full diagram. Using the present analysis, a full phase diagram can still be determined. Whereas for the other examples in Figs. 9 and 10(a–c) the experimental tie-lines serve as a check on the quality of the fit, this is not the case for Fig. 10(d) and the phase diagram should be considered to be a prediction.

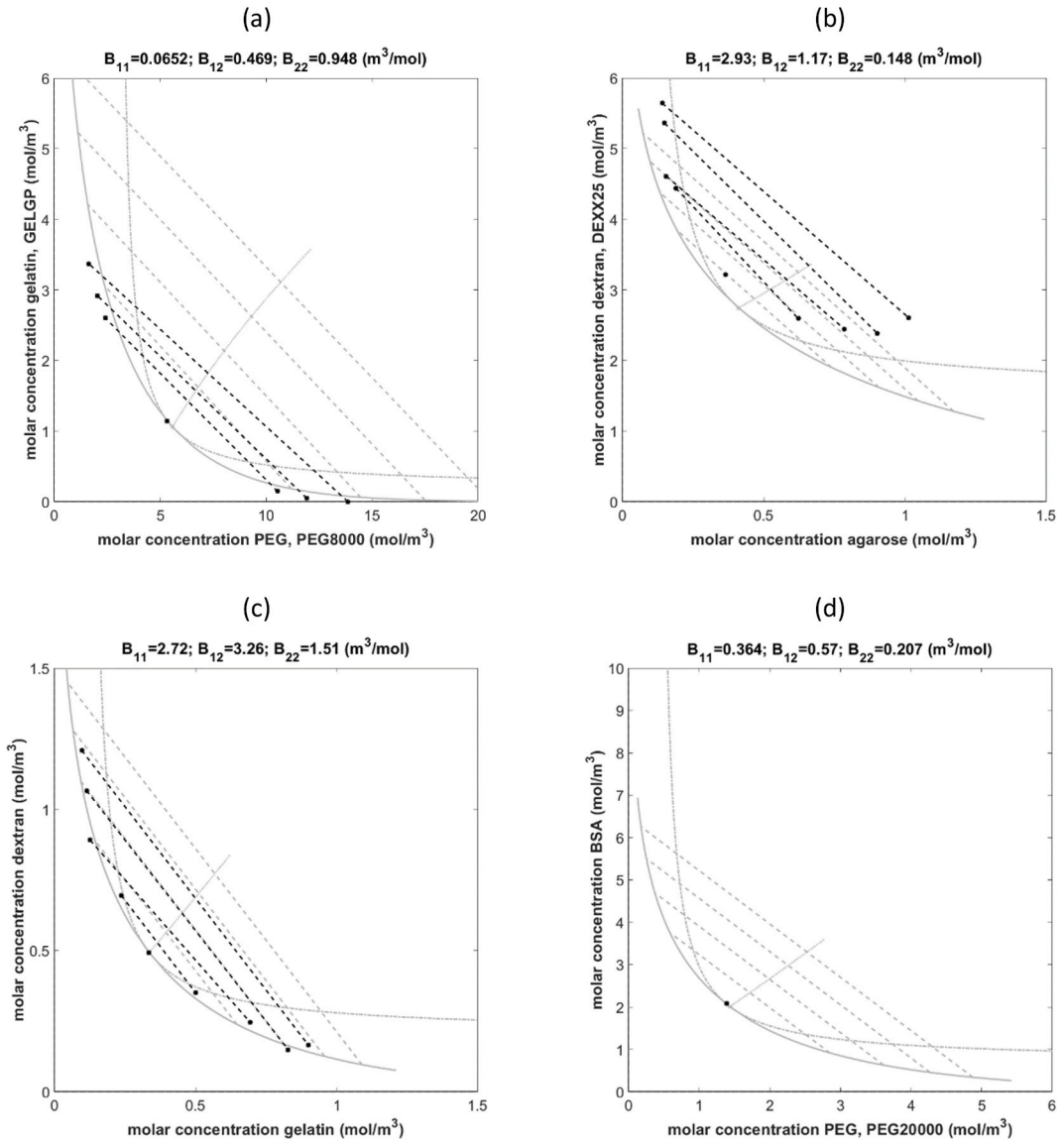

Fig. 10. Phase diagram for (a) PEG8000 + porcine gelatin at 50 °C by Lee et al. (2020); (b) agarose + DEXX25 at 80 °C by Medin and Janson (1993); (c) gelatin + dextran at 50 °C by Edelman, Tromp, and van der Linden (2003); (d) PEG20000 + BSA at 28 °C by Edmond and Ogston (1968): (black) experimental data; (grey) present fit; (solid line) binodal; (dash-dotted line) spinodal; (dashed line) tie-lines; (dotted line) midpoints of tie-lines; (●) critical points and end-points of experimental tie-lines. For the virial coefficients mentioned in the header, component '1' is plotted along the horizontal axis, whereas component '2' is plotted along the vertical axis.

6. Conclusions

The present results demonstrate that it is possible to use literature data on the critical point in the phase diagram of biopolymer mixtures to build a database of second virial coefficients if these published phase diagrams contain shared components. If no shared components are present, the assumption of relations between the second virial coefficients (e.g. a power-law dependence on the molecular weight) can create relations between the second virial coefficients for the components. Note that the benefit of using the critical point is that polydispersity of the sample will not lead to fractionation, so the second virial coefficients that are obtained reflect a fair weighing of all components in the mixture.

The method described in this paper has become practical thanks to the earlier derived analytical expressions for the critical point (Dewi et al., 2020; Bot et al., 2021a). Previously, the fitting used in this paper would have been a theoretical possibility, but the speed of the calculation would have been reduced by the more extensive numerical evaluations that would have been required. By simultaneously fitting multiple phase diagrams it was possible to avoid the pitfalls identified by Clark (2000).

It was confirmed that the second virial coefficients of dextran that were derived from membrane osmometry match the ones obtained from the analysis of literature data quite well, in particular for the molecular weight dependence. This is especially surprising if one takes into consideration that the method used to obtain these second virial coefficients is radically different. It should also be realized that the experimental results from the literature that have been analyzed in this paper have not been obtained using exactly the same protocol, and therefore the data may not be fully comparable. Depending on the desired accuracy, this may or may not be acceptable. To understand the impact of molecular weight on the second virial coefficient, the approach seems sufficiently accurate, but to extract the more subtle effect of temperature, the data from the literature seems insufficiently accurate.

Also, it was shown for the mixtures studied that a simple (approxi-

mate) mixing rule for second virial coefficients could be identified, which expresses B_{12} in terms of B_{11} and B_{22}. The mixing rule was found to work particularly well when $B_{12} > 1\ m^3/mol$. It is expected that this will hold for polymer mixtures that mainly interact through their excluded volumes. This mixing rule opens the opportunity to estimate the phase diagram for polymer mixtures from a database (like Table 1 or Table 2) without knowing their cross-virial coefficient.

The method described in this paper can applied to additional phase diagrams that were published already in the literature or newly obtained ones, provided that the data sets contain a sufficient number of shared components, either within the new set or within the already analyzed phase diagrams. As such, one could envisage the current set of systems as the seed for a growing database of virial coefficients. This will allow the predictions for the phase diagrams of an ever-increasing number of biopolymer combinations.

It should be noted that the fact that the phase diagrams match reasonably well but not perfectly is good enough for many practical situations in for example product development, as two-component phase diagrams are anyhow somewhat of an idealization of the real complex situation at hand (which involve more complicated mixtures of less well-defined ingredients) (e.g. Bot et al., 2014). In such situations a more accurate prediction is desired but not required, and any reasonable prediction is preferred over no prediction.

CRediT authorship contribution statement

Arjen Bot: Conceptualization, Methodology, Software, Writing – original draft, Visualization, Investigation, Supervision. **Belinda P.C. Dewi:** Investigation, Writing – original draft. **Titia Kool:** Investigation. **Erik van der Linden:** Conceptualization, Supervision. **Paul Venema:** Conceptualization, Methodology, Software, Writing – original draft, Visualization, Investigation, Supervision.

Declaration of competing interest

The authors declare that no competing interests exist in relation to this manuscript.

Acknowledgement

Belinda P.C. Dewi acknowledges financial support by the Indonesia Endowment Fund for Education (LPDP-Lembaga Pengelola Dana Pendidikan) scholarship, Ministry of Finance, The Republic of Indonesia.

References

Albertsson, P. A. (1986). *Partition of cell particles and macromolecules* (3rd ed.). New York: Wiley.

Bot, A., Dewi, B. P. C., & Venema, P. (2021a). Phase-separating binary polymer mixtures: The degeneracy of the virial coefficients and their extraction from phase diagrams. *ACS Omega, 6*, 7862–7878.

Bot, A., Dewi, B. P. C., & Venema, P. (2021b). Addition to "Phase-separating binary polymer mixtures: The degeneracy of the virial coefficients and their extraction from phase diagrams". *ACS Omega, 6*, 20086–20087.

Bot, A., Foster, T. J., & Lundin, L. (2014). Modelling acidified emulsion gels as Matryoshka composites: Firmness and syneresis. *Food Hydrocolloids, 34*, 88–97.

Clark, A. H. (2000). Direct analysis of experimental tie line data (two polymer–one solvent systems) using Flory–Huggins theory. *Carbohydrate Polymers, 42*, 337–351.

Connemann, M., Gaube, J., Leffrang, U., Müller, S., & Pfennig, A. (1991). Phase equilibria in the system poly(ethylene glycol) + dextran + water. *Journal of Chemical & Engineering Data, 36*, 446–448.

Dewi, B. P. C., van der Linden, E., Bot, A., & Venema, P. (2020). Second order virial coefficients from phase diagrams. *Food Hydrocolloids, 101*, Article 105546.

Dewi, B. P. C., van der Linden, E., Bot, A., & Venema, P. (2021). Corrigendum to "Second order virial coefficients from phase diagrams". *Food Hydrocolloids, 112*, Article 106324.

Diamond, A. D., & Hsu, J. T. (1989a). Fundamental studies of biomolecule partitioning in aqueous two-phase systems. *Biotechnology and Bioengineering, 34*, 1000–1014.

Diamond, A. D., & Hsu, J. T. (1989b). Phase diagrams for dextran-PEG aqueous two-phase systems at 22°C. *Biotechnology Techniques, 3*, 119–124.

Doi, M., & Edwards, S. (1986). *The theory of polymer dynamics*. New York: Clarendon Press, Oxford University Press.

Edelman, M. W., Tromp, R. H., & van der Linden, E. (2003b). Phase separation-induced fractionation in molar mass in aqueous mixtures of gelatin and dextran. *Physical Review E, 67*, Article 021404.

Edelman, M. W., van der Linden, E., & Tromp, R. H. (2003a). Phase separation of aqueous mixtures of poly(ethylene oxide) and dextran. *Macromolecules, 36*, 7783–7790.

Edmond, E., & Ogston, A. G. (1968). An approach to the study of phase separation in ternary aqueous systems. *Biochemical Journal, 109*, 569–576.

Ersch, C., van der Linden, E., Martin, A., & Venema, P. (2016). Interactions in protein mixtures. Part II: A virial approach to predict phase behaviour. *Food Hydrocolloids, 52*, 991–1002.

Esquena, J. (2016). Water-in-water (W/W) emulsions. *Current Opinion in Colloid & Interface Science, 25*, 109–119.

Forciniti, D., Hall, C. K., & Kula, M. R. (1991). Influence of polymer molecular weight and temperature on phase composition in aqueous two-phase systems. *Fluid Phase Equilibria, 61*, 243–262.

Furuya, T., Iwai, Y., Tanaka, Y., Uchida, H., Yamada, S., & Arai, Y. (1995). Measurement and correlation of liquid-liquid equilibria for dextran-poly(ethylene glycol)-water aqueous two-phase systems at 20°C. *Fluid Phase Equilibria, 103*, 119–141.

Ghosh, S., Vijayalakshmi, R., & Swaminathan, T. (2004). Evaluation of an alternative source of dextran as a phase forming polymer for aqueous two-phase extractive system. *Biochemical Engineering Journal, 21*, 241–252.

Lee, J. M., Chan, E. S., Nagasundara Ramanan, R., & Ooi, C. W. (2020). Liquid-liquid equilibria of aqueous two-phase systems made of polyethylene glycol and gelatin systems and their application in emulsion formation. *Fluid Phase Equilibria, 508*, Article 112441.

McMillan, W. G., & Mayer, J. E. (1945). The statistical mechanics of multicomponent systems. *The Journal of Chemical Physics, 13*, 276–305.

Medin, A. S., & Janson, J. C. (1993). Studies on aqueous polymer two-phase systems containing agarose. *Carbohydrate Polymers, 22*, 127–136.

Rohatgi, A. (2021). *WebPlotDigitizer* Accessed Nov, 20th, 2021 https://automeris.io/WebPlotDigitizer/.

Semenova, M. G. (2018). Equilibrium in Colloidal systems. In C. Gambini Pereira (Ed.), *Thermodynamics of phase Equilibria in food Engineering* (pp. 507–528). Cambridge, MA: Academic Press.

Sturtewagen, L., & van der Linden, E. (2021). Effects of polydispersity on the phase behavior of additive hard spheres in solution. *Molecules, 26*, 1543.

Tolstoguzov, V. B. (1991). Functional properties of food proteins and role of protein-polysaccharide interaction. *Food Hydrocolloids, 4*, 429–468.

Vink, H. (1971). Precision measurements of osmotic pressure in concentrated polymer solutions. *European Polymer Journal, 7*, 1411–1419.

Zaslavsky, B. Y., Bagirov, T. O., Borovskaya, A. A., Gulaeva, N. D., Miheeva, L. H., Mahmudov, A. U., & Rodnikova, M. N. (1989). Structure of water as a key factor of phase separation in aqueous mixtures of two non-ionic polymers. *Polymer, 30*, 2104–2111.